Rayleigh-Taylor mixing may account for the position anomaly in NIF dot experiments

Olivier Poujade, M.A. Barrios, S. D. Baton, Christophe Blancard, Ronan Devriendt, Michel Primout

▶ **To cite this version:**

Olivier Poujade, M.A. Barrios, S. D. Baton, Christophe Blancard, Ronan Devriendt, et al.. Rayleigh-Taylor mixing may account for the position anomaly in NIF dot experiments. Physics of Plasmas, 2021, 28, pp.042704. ⟨10.1063/5.0040583⟩. ⟨hal-03080023⟩

HAL Id: hal-03080023

https://hal.science/hal-03080023v1

Submitted on 17 Dec 2020

HAL is a multi-disciplinary open access archive for the deposit and dissemination of scientific research documents, whether they are published or not. The documents may come from teaching and research institutions in France or abroad, or from public or private research centers.

L'archive ouverte pluridisciplinaire **HAL**, est destinée au dépôt et à la diffusion de documents scientifiques de niveau recherche, publiés ou non, émanant des établissements d'enseignement et de recherche français ou étrangers, des laboratoires publics ou privés.

HAL Authorization

Rayleigh-Taylor mixing may account for the position anomaly in NIF dot experiments

O. Poujade,[1,2,a)] M. A. Barrios,[3] S. Baton,[4] C. Blancard,[1,2] R. Devriendt,[1] and M. Primout[1]
[1)] *CEA, DAM, DIF, F-91297 Arpajon, France*
[2)] *Université Paris-Saclay, CEA, LMCE, F-91680, Bruyères-le-Châtel, France*
[3)] *Lawrence Livermore National Laboratory, Livermore, California 94551, USA*
[4)] *LULI-CNRS-CEA-Ecole Polytechnique, F-91128 Palaiseau cedex, France*

(Dated: 15 December 2020)

The "dot spectroscopy" experiment[2,3] allows for a simultaneous measurement of the electron temperature (T_e) and position of a patch of Mn and Co inside a hohlraum, as described by Barrios et al[2]. HYDRA simulations systematically predicted a dot location further away from it's starting location than observed in the experiment. In the article, integrated hydro-rad simulations with TROLL have led to the same trend as HYDRA. A new ad-hoc treatment of laser absorption, through what we have called *absorption multipliers*, has been implemented in TROLL in order to mimic the effect of absorption mechanisms other than inverse-Bremsstrahlung. It led to the instrumental conclusion that whatever physical phenomenon was responsible for the position anomaly must have occurred in the early stage. More precise simulations of the dot region, from early to late time, show that the position discrepancy can be explained by a Rayleigh-Taylor mixing of the dot into the ablator as it expands in the hohlraum. This mixing tends to shift the simulated dot closer to the location measured in the experiment. But, the mixing also changes the interpretation of the electron temperature from the spectral line ratios.

I. INTRODUCTION

For over ten years, progress toward ignition has been slow using the indirect-drive technique of inertial confinement fusion (ICF) on the National Ignition Facility (NIF). It consists in making the totality of the 192 NIF intense UV-laser-beams to be converted into X-rays into a centimeter-sized gold hohlraum at the centre of which lies a millimeter-sized DT capsule. The approximately uniform and isotropic bath of x-rays, resulting from that conversion, irradiates the surface of the capsule and is responsible for the outward ablation of its outer shell which, in turn, triggers the capsule interior implosion in order to achieve plasma alpha-heating[20] and ignition conditions[9,21].

In order to accomplish that succession of events with precise enough timing, strength and stability, a sharp understanding of complex physical processes happening in the laser heated plasma within the hohlraum[32] is required. Among these processes stand in good position hydrodynamic instabilities, kinetic effects, laser-plasma instabilities, non local thermal equilibrium (NLTE) atomic physics and electrons transport (conduction).

Hydrodynamic instabilities[8,19,31,35,48] can be due to irradiation non uniformity of the capsule, they can also be due to surface defects or even molecular composition inhomogeneities[1] on the outer surface of the ablator.

Kinetic effects[40] within the hohlraum might have sizeable consequences but are still way to complex to take into account in hydro-radiation simulation codes.

Laser-plasma instabilities (LPI)[25,46] take place in gas filled hohlraum at the laser entrance hole (LEH) but also deeper in the hohlraum when laser beams interact with gold-wall bubbles. In situations where LPI are not expected to have much importance, such as short pulse drives in near vacuum hohlraums (NVH)[4], experimental results compare well to numerical simulations with radiation-hydro-code such as HYDRA or TROLL[13,27]. NVH experiments have demonstrated improved laser-hohlraum coupling with much less backscatter than gas-filled hohlraums. Phenomenological drive multipliers are close to unity[6] in NVH ($\sim$0.9). On the contrary, when LPI matter, for long pulse drives in gas-filled hohlraums[23], there is a glaring discrepancy with numerical simulations predicting stronger drives over experiments. Drive multipliers close to 0.75 are required to reach a reasonable agreement with experiment.

Non local thermal equilibrium (NLTE) atomic physics is of the essence[24] when it comes to modelling emissivity of gold wall in a hohlraum. The majority of the x-ray emission comes from a thin layer ($\sim$ 100 μm) of ablated gold wall at the onset of $T_e \neq T_r$. In this region, the competition between collision and radiation, that strongly depends upon T_e, needs to be precisely modelled.

Finally, the description of electron thermal transport is instrumental in the distribution of T_e within the hohlraum. Electrons being the lighter particles of matter in an ICF plasma, they are also the more mobile and can easily evacuate heat from a location and heat up neighbouring regions depending on the intensity of the conduction mechanism. This is the reason why it can have important consequences on simulations[24] depending upon the way it is modelled, using local or non-local closure.

To summarize, the understanding and modelling of many physical domains of paramount importance to the working of a hohlraum still need to be improved.

[a)] Electronic mail: olivier.poujade@cea.fr (corresponding author)

In order to grasp what is missing in the plasma modelling implemented in radiation-hydro-codes, it was realized that the laser driven plasma needed to be characterized *in situ*. Many physical quantities are needed in order to describe a macroscopic plasma, locally, in an unambiguous manner. Among all these quantities, a few are always referred to when comparing plasmas such as: the electron density (n_e), the degree of ionization (Z^*) and the electron temperature (T_e). The dot spectroscopy platform[2,3] was developed in this context in order to assess one of these quantities: the electron temperature of the plasma within the hohlraum.

The basic principle behind these dot spectroscopy platforms on NIF is as follow : a tracer-dot of Mn:Co is deposited either on the outer surface of the target ablator, in the *dot-on-capsule*[2,3] experiment (at the pole or at the equator), or suspended on a film between the capsule and the LEH, in the *dot-on-film* experiment. In both cases, two time resolved diagnostics are deployed. The first one is a framing camera that is set up to spatially locate the dot as the experiment unfolds. The second one is an x-ray spectrometer[34] (between 6 and 8 keV) to observe the emission of the dot during the operation of the platform.

The one-to-one relation between adequate spectral line-ratios, of Mn and Co, and the dot electronic temperature T_e was evaluated using a detailed atomic physics code such as SCRAM[2]. Using this relation to infer the experimental electronic temperature, all dot experiment, so far, have consistently shown that the peak T_e was higher in the experiments (by $\sim$500 eV) than in simulations[2] and experimental trajectories were different by few hundred microns compared to the simulations with HYDRA (the experimental dot being slower than the simulated dot). Here, we report on a similar trend with CEA's hydro-radiation-code TROLL[13,27].

This article will focus on the hydrodynamic evolution of the dot experiment N141216 (0.8$\times$ scaled hohlraum, gas filled with C_5H_{12} at 1.37 mg/cm^3) to explain the discrepancy with simulation reported in Barrios[2,3]. The possibility of a mixing between the tracer-dot and the ablator is advocated on theoretical grounds and supported with numerical simulations.

So far, all simulations of this platform (with HYDRA at LLNL or with TROLL at CEA) were integrated and the possibility of a mixing was largely inhibited by the coarse resolution of these simulations. Refined simulations of the region around the tracer-dot and the ablator, subjected to the correct irradiation versus time, have shown that mixing might occur very early in the course of the drive and would be caused by classical Rayleigh-Taylor instability at the interface between the tracer-dot and the ablator. This effect seems to be enough to reconcile simulations and experiments with respect to the dot location versus time (different by $\sim$200 μm).

A brief description of the dot experiment along with the main results obtained is given in section II. The exact same simulation has been carried out with TROLL. The 2D integrated simulation setup and the results concerning the hydrodynamic evolution of the dot is reported in section III. Absorption mechanism in a large sense have been pushed forward as the cause of these discrepancies. A modelling alternative, by means of *absorption multipliers*, is presented in section IV and results and discussion on the trajectory of the dot follows in section V where various possibilities to reconcile simulations and experiment are considered.

The main conclusion is that, whatever caused the slowing down of the dot in the experiment had to be doing it from a very early stage of the evolution.

The acceleration profile of the dot/ablator interface is such that a classical Rayleigh-Taylor (as opposed to ablative RT) instability can take place. A 2D plane simulation, representative of the integrated simulation in terms of irradiation, is described in section VI where the evolution of a defect-less interface is made to move as in the integrated simulations by shaping the radiative temperature (T_r) history. Using the very same T_r-law to simulate the evolution of the dot with a realistic dot/ablator interface perturbation, it is possible to show that the dot mixes with the ablator and sinks into it, shifting its location towards the centre of the platform as observed in the experiment.

Finally, in section VII, the potential consequences of the dot-ablator mixing over spectral measurements is discussed and in particular the evaluation of electronic temperature through the measurement of the spectral line ratios described in the articles by Barrios et. al.[2,3].

II. DESCRIPTION OF THE DOT EXPERIMENT

The dot-spectroscopy experiment uses a viewfactor[30] platform, which is normally used for its versatility when concerned with diagnostic, but was used here to reduce the gold emission background from the LEH[42]. The top end of the hohlraum in Fig.1 is a regular laser entrance hole (LEH). At the bottom end, on the contrary, the LEH has been removed in order to have a good view on the inside of the hohlraum.

The dot is a very thin patch (1600 Å or 3200 Å) of Mn:Co (at 50-50 % atomic concentration) deposited on the outer surface of the ablator to act (i) as a passive tracer to locate this ablated outer surface as time goes by and (ii) as a passive sensor whose emission supplies information about the plasma state and the electronic temperature (T_e) at the location of the dot.

A slit has been made along the gold hohlraum in order to observe (side-on) the motion of the dot with a streaked camera. Moreover, a temporally resolved x-ray spectrometer was located on the axis of the experiment in order to measure (head-on) the emissivity spectrum of the dot for photons energies between 6 and 7 keV through the laser-entrance-hole (LEH). That particular spectral band is interesting for the targeted plasma state (between T_e=3 and 5 keV) for it provides various emission lines whose intensity ratios can be mapped through

a one-to-one relation to the electronic temperature.

This relation, between line ratios and T_e was evaluated with the detailed atomic code SCRAM[2]. Two important assumptions behind this evaluation are of the essence (apart from the fact that the atomic code must be trusted). First, the electron distributions are Maxwellian (which is not obvious for a dot travelling through a bunch of very intense laser beams). Second, the relation between line ratios and T_e should be insensitive to n_e, as reported in the original dot article[2], and to the dot thickness which is poorly measured experimentally. This matter will be discussed in section VII.

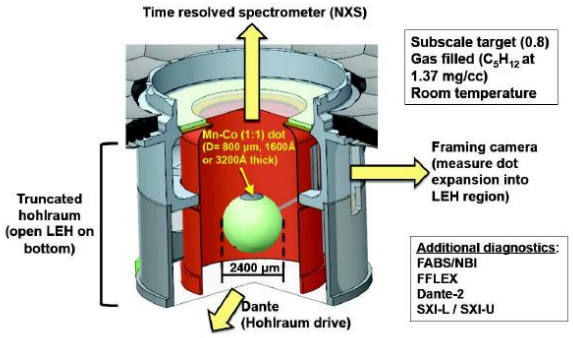

FIG. 1. Schematic of the dot-on-capsule experiment. A patch of Mn:Co deposited on the outer surface of a spherical target is used as a passive tracer to measure the expansion of the ablator plasma (with a framing camera on the side) and to measure the electron temperature at the different locations crossed by the dot (with a time resolved spectrometer).

III. 2D INTEGRATED SIMULATIONS

Full 2D axisymmetric integrated simulations of the dot experiment have been carried out with the radiation transfer code TROLL[13,27]. QSEM[12,22,38] equations of state have been used to model the gold wall, the dot deposited on the capsule and the ablator. A QSEM equation of state is a sophisticated set of different models. It is an average atom-model where the electron part comes from a fully quantum calculation and the cold curve is provided by experimental data or calculated by quantum molecular dynamics (QMD), the ion part being the classical Cowan ion equation of state[33] .

Because of the small thickness of the dot (1600 Å) on the surface of the ablator compared to the overall size of the experiment the meshing is an important issue[15]. A reasonable amount of mesh needs to be kept in the dot as it expands during the drive. It is customary to adapt the size of the mesh at an interface in such a way that the mass within a mesh remains roughly constant through the interface. This is why, in a heavy material in contact with a light material, the size of the mesh should be much smaller (in proportion to the density ratio). This is to avoid spurious numerical effects related to unphysical transmitted or reflected compression waves, rarefactions or shocks.

Another problem has to do with the way the dot is meshed along the polar angle. In order to correctly describe the spherical surface of the capsule a 2 degrees sampling is enough which correspond, at the outer radius of the capsule (1 mm) to 35 μm, to be compared to the 0.16 μm radially. This strong aspect ratio is not a good thing numerically when it comes to vorticity motion in the flow. Indeed, in such situation, cells are distorted by the dragging flow up to a point where they get tangled up and not convex anymore. The use of a pure Lagrange scheme, which would be the ideal solution to trace the material of the dot through the whole simulation, is made quite difficult.

One has to resort to an ALE[13,27] scheme which is more versatile and robust with respect to the mesh inhomogeneity. The drawback is that material in the cells at the contact line diffuse in the neighbouring cells of the other material on the other side of the line. It occurs at every single time-step of the simulation owing to the remap phase of any ALE scheme. This numerical diffusion tends to make the thickness of the evolving dot larger than it should. One way to overcome this issue is to finely mesh the dot in order to reduce that effective diffusion.

We have tested three meshes for the *dot* (cf. Tab.I) in order to limit the diffusion without expanding too much the number of mesh in our fully integrated simulations to keep the calculation cost reasonable.

mesh id	# layers thickness	# layers diameter
M1	4	4
M2	20	6
M3	40	10
Farmer[15]	10	14

TABLE I. Various discretization of the dot (M1, M2 and M3) in simulations using TROLL compared to the discretization used in HYDRA in Farmer[15].

Increasing the number of meshes in one region of the simulations is not innocuous for it has knock-on effects on other connected regions. This is the reason why, even if the number of mesh variation between M2 ($20\times6=120$) and M3 ($40\times10=400$) do not seem important, its consequences on connected regions of the integrated simulation can be overwhelming. This is the main limiting factor in the meshing of the dot (along with high aspect ratios).

The lesson of this comparison is that there is a clear difference in the dot behaviour between the M1 and M2 simulations that fades out between M2 and M3. We cannot honestly talk about a converged mesh at M3 but it is the closest to converged we can reasonably get. The same kind of meshing was provided in Farmer's[15] simulations. In the remainder of this article, simulations we are referring to were carried out with M3.

IV. SIMPLE MODELLING OF VARIOUS ABSORPTION MECHANISM

Taking into account all effects contributing to absorption in a HED plasma (inverse bremsstrahlung, laser plasma instabilities, Raman scattering, Brillouin scattering, cross beam energy transfer) is still out of reach for present simulation codes (TROLL, LASNEX, HYDRA).

Yet, one should not ignore these effects on the pretext that one cannot simulate them. Two methods have been developed in the ICF literature to overcome these excruciating issues: *power multipliers* (PM) and *enhanced propagation* (EP).

(PM) – One way to artificially alter laser absorption is to modify the incoming laser power by using what has been called *power multipliers*[23,28,29,41] throughout the NIC campaign. These multipliers vary with time and affect the power delivered by the laser beams to the hohlraum. In general, there are two time-varying multipliers, one affected to the inner beams and the other one to the outer beams. This strategy has been used, and is still in use, to match VISAR shock velocity measurement and/or to match experimental symmetry of the hot-spot (as a way to take into account energy transfer between inners and outers through CBET and backscattered energy due to laser-plasma instability).

(EP) – Another way to artificially alter laser absorption in simulations is to modify the laser frequency[5,47].The bigger the frequency, the smaller the absorption. That method has been used to increase propagation[5] of the inner beams in simulations (*enhanced propagation simulations*) in order to adjust the post-shot modelling of the symmetry of implosion which was oblate at 3ω and turned prolate at 5ω as observed experimentally. This method was investigated further[47] and applied to both inner and outer beams with higher frequencies of 5 or 9ω for the inners and lower frequency of 2ω for the outers.

The drawback with this method is that the position of the critical surface is modified along with the laser beam trajectory because the refractive index also depends upon frequency

$$n = \sqrt{1-\omega_p^2/\omega^2}. \tag{1}$$

This is why, we have resorted to yet another ad-hoc numerical technique called *absorption multipliers* (AM).

(AM) – The *absorption multipliers* technique affects absorption by letting the full laser energy inside the hohlraum, unlike method (PM), and without altering critical surface and index of refraction, contrary to method (EP).

In a simple Drude model, absorption coefficient μ depends upon laser frequency ω, plasma frequency $\omega_p = (e^2\, n_e/\varepsilon_0\, m_e)^{1/2}$, and electron-ion momentum collision frequency

$$\nu_{ei} = \frac{4\sqrt{2\pi}\, e^4}{3\,(4\pi\varepsilon_0)^2\sqrt{m_e}}\,\frac{n_e}{(k_B\,T)^{3/2}}\,Z^*\,\ln\Lambda\,, \tag{2}$$

in such a way that

$$\mu = \frac{\nu_{ei}}{c}\,\frac{\omega_p^2}{\omega^2}\,\frac{1}{\sqrt{1-\omega_p^2/\omega^2}}\,, \tag{3}$$

and beam power loss $\mathrm{d}I(s)$ in matter, after travelling a distance $\mathrm{d}s$, is

$$\mathrm{d}I(s) = -\mu\, I(s)\,\mathrm{d}s\,. \tag{4}$$

As can be noticed, absorption involves dissipative phenomenons such as collisions. Refraction, on the contrary, involves mostly non-dissipative collective phenomena such as plasma oscillations. One should be allowed to modify absorption (because of our lack of understanding of these irreversible processes) and keep the (more simple) phenomenology of refractive index unchanged.

In order to circumvent that issue, a modification of eq.(3) was implemented in TROLL. An adjustable constant, C_{abs}, called an *absorption multiplier*, as opposed to *power multiplier*, was grafted to the right hand side of eq.(3) so that

$$\mu = C_{\mathrm{abs}}[\mathrm{mat}]\,\frac{\nu_{ei}}{c}\,\frac{\omega_p^2}{\omega^2}\,\frac{1}{\sqrt{1-\omega_p^2/\omega^2}}\,. \tag{5}$$

We allowed the possibility for different values of $C_{\mathrm{abs}}[\mathrm{mat}]$ in different materials ([mat] in eq.(5)) in order to grasp the influence of a modified absorption on simulations outcomes. The effect of C_{abs}, as we can see from eq.(4), is to multiply the laser absorption per unit length by a factor C_{abs} which can be used either to enhance propagation (if < 1) or to reduce propagation (if > 1).

A constant C_{abs} in front of μ is not at all equivalent to modifying the laser frequency. Of course, one could argue that a convenient choice of $\omega \neq \omega_L$ in EP (corresponding to $C_{\mathrm{abs}} = 1$) could get us to the same value of μ than AM with $\omega = \omega_L$ and $C_{\mathrm{abs}} \neq 1$. Problem with EP is that $\omega \neq \omega_L$ involves a modification of the index of refraction n in eq.(1). AM on the contrary, does not affect the index of refraction nor the critical density $n_c = \varepsilon_0\, m_e\, \omega^2/e^2$. It does not alter refraction and it only modifies the way the beam is absorbed along its trajectory and up to the critical density surface.

The benefit of an *absorption multiplier* (in a given material) is twofold. First, it allows to encapsulate, in an effective constant, our lack of knowledge of the inverse bremsstrahlung absorption mechanism due to collective effects (summed up in the coulombian logarithm's renowned variability in the literature) or to kinetic effects (if velocity distributions are not Maxwellian, the prefactor in eq.(2) can substantially be modified[26]). Second,

it provides a useful knob to move the absorption region within the hohlraum along the trajectory of laser beams. Therefore, even if the inverse bremsstrahlung mechanism is thought to behave as predicted by eq.(2) in a specific plasma, in which case one would be drawn to set $C_{\rm abs} = 1$, other absorption mechanisms at play, which are poorly or not simulated by hydrorad codes (laser-plasma-instabilities, CBET, etc), can be mimicked by $C_{\rm abs} > 1$, in the gas-fill for instance, to keep a strong absorption close to the LEH, or by a $C_{\rm abs} < 1$, on the contrary, to enhance propagation.

The diversity of scenarios spanned by the variation of these *absorption multipliers*, keeping the oncoming energy into the hohlraum unchanged, was paramount in pointing out that whatever causes the position anomaly must have occurred at very early stage as will be demonstrated in the following section.

V. DISCREPANCY IN THE DOT POSITION BETWEEN SIMULATIONS AND EXPERIMENTS

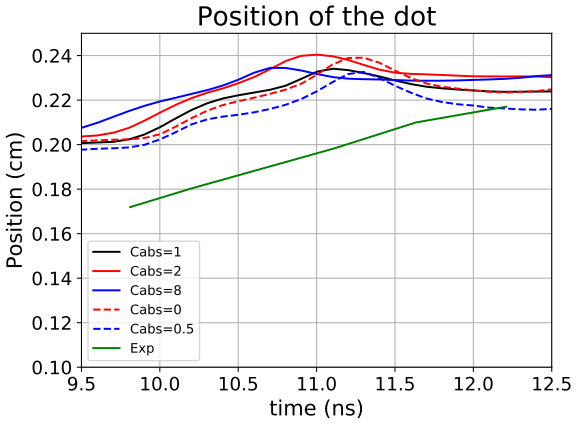

FIG. 2. Simulated position of the dot for various values of $C_{\rm abs}$ (the value 1 correspond to the regular inverse bremsstrahlung). Values less than 1 correspond to a less absorbed laser that will deposit less energy in the gas and will carry more of its energy to the wall. Values more than 1 correspond to a more absorbed laser energy in the gas and less energy reaching the gold wall. Whatever the value of $C_{\rm abs}$ simulations are shifted consistently by 300 μm with respect to the experimental data which is unexplained so far.

Experimental positions of the dot at various instant are reported in Fig.2. The averaged position of the dot, or the average of any physical quantity (let us call it Ψ) for that matter, is defined using the squared electron density[15] as a weight function in such a way that

$$\overline{\Psi}_{\rm dot}(t) = \frac{\int_{V_{\rm dot}} n_e^2(\boldsymbol{x},t)\,\Psi(\boldsymbol{x},t)\,{\rm d}^3x}{\int_{V_{\rm dot}} n_e^2(\boldsymbol{x},t)\,{\rm d}^3x}, \qquad (6)$$

because x-ray emission is proportional to $n_e\,n_i \sim n_e^2$.

As one can see in Fig.2, the simulated trajectory is off by approximately 300 μm whatever the AM simulations and values of $C_{\rm abs}$ chosen (more or less absorbing). Moreover, the velocity of the dot (~ 150 km/s), assessed by the slope of both trajectories, is similar between simulations and experiments but positions disagree. One hypothesis is that the dot trajectory at early times is wrong which leads to a later time offset in dot position. It is also possible that there is a strong late time acceleration which is different between the simulation and experiment.

If one zooms out of the late stage of the trajectory (depicted on Fig.2) and take a look at the broader view of the whole history given by Fig.3 new scenarios can emerge.

Indeed, the simulated trajectories showed no dependence on $C_{\rm abs}$ and no significant event occurring between 0 and 10 ns apart from the initial acceleration. Compression/shock waves, coming from the expanding gold bubbles or from the gas-fill blown off by the laser, cross the trajectory of the dot during its motion but they do not significantly affect its course as we will show next.

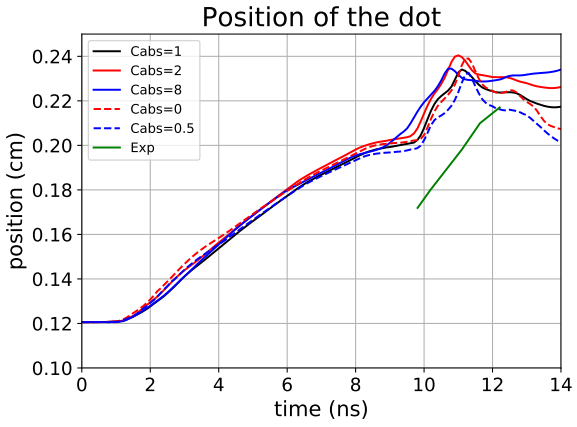

FIG. 3. Simulated position of the dot is independent of $C_{\rm abs}$ values used up until 9 ns. It is difficult to explain how the trajectory could go from 0.2 cm at 9 ns to 0.17 cm at 10 ns. So, whatever should explain the discrepancy with the experiment should start very early in the course of the experiment for the trajectory to be less steep between 2 and 8 ns than currently simulated.

It can be inferred from Fig.3 that once the dot has been accelerated between 0 and 2 ns, its trajectory is almost ballistic from 2 to 9 ns before being reaccelerated by the final laser pulse between 9 ns and 10 ns (see Fig.3). This implies that, between 0 and 2 ns, the acceleration of the experimental dot must be smaller to explain a shorter final distance travelled by the dot. We have been unable to find a value of $C_{\rm abs}$ which gives the dot a weaker initial acceleration which is also consistent with other experimental observables. What is crucial here is the fact that, whatever the value of $C_{\rm abs}$, that is to say whatever the hohlraum scenario, as long as the drive is kept unchanged, the trajectory, velocity and acceleration

(although it is noisier than the former two) remains the same at early stage (< 9 ns).

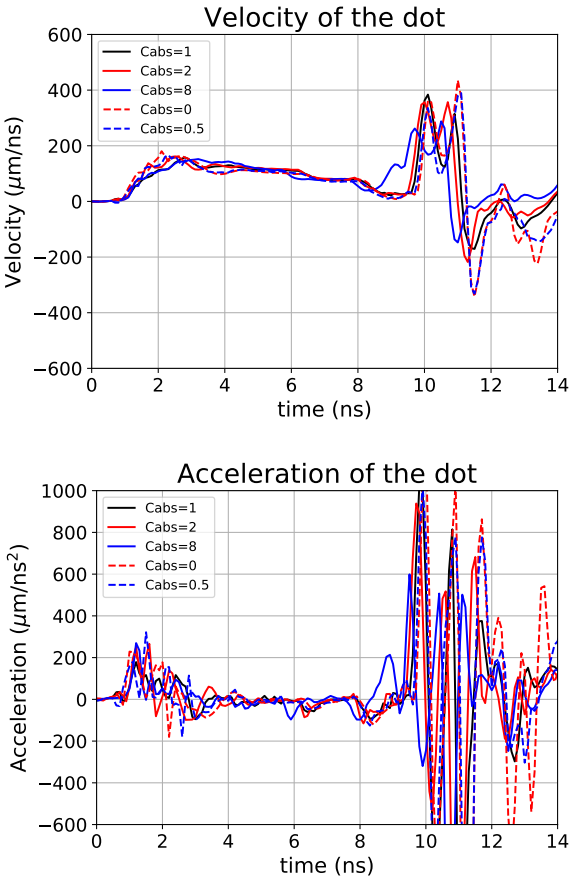

FIG. 4. Velocity and acceleration of the dot as time goes by (derived by taking the time and second time derivative of the dot position). Velocity histories are equivalent up until 8 ns in agreement with position histories. There are two strong mostly positive acceleration phases quite noticeable, between 1 and 2 ns and starting at 9 ns, on the noisy acceleration history (due to the fact it is a second derivative). The positive acceleration means a push directed outward from the capsule. In the dot reference frame, it is equivalent to a gravity directed inward.

This is the important result where *absorption multipliers* have been instrumental: all physics effects, that can be approximated as an absorption of the laser, cannot exert any leverage on what happens at early stage (cf. Fig.3) and, in the late stage of the experiment (> 9 ns), where all sorts of missing physics could clearly affect the trajectory, all seems to pin down to the fact that if one tries to move the trajectory of the dot away from its anomalous location, by adjusting various knobs, it has unreasonable consequences (higher T_e, more glint[15], etc). This is the reason that brought us to look for an early cause of this anomalous position of the dot.

Adjusting different knobs to make simulations match the experiment – only makes sense as long as the dot keeps, more or less, the shape predicted by these integrated simulations, and precisely, these very integrated simulations do predict that the dot travels and expands experiencing nothing more than plain advection with the ablator. A part or all of these effects (value of f, LPI, NLTE, etc), as part of a multifactorial cause, might contribute, to a certain extent, to the anomalous position if the dot's integrity is unaffected. But what if the dot were to experience a drastically different hydrodynamics such as mixing with the ablator ?

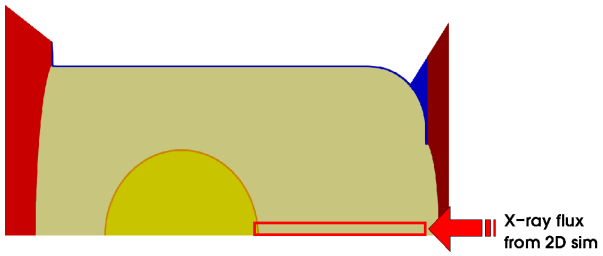

FIG. 5. (a) Schematic of the dot experiment as modelled in our integrated TROLL simulations. The red frame corresponds to the part of the integrated simulation that is the object of a dedicated hydrorad simulations to assess the importance of hydrodynamics instabilities on the dot. (b) It is a one wavelength simulations with $\lambda = 10$ μm (corresponding to the width of the simulation) and initial amplitude of $a(\lambda) = 0.1$ μm. The simulation is 2.7 mm long from the centre of the capsule towards the LEH. X-ray flux is extracted from the integrated simulation and fed to the dedicated simulation through a time varying flux law on the right boundary.

A closer look at the acceleration history of the dot, Fig.4, shows two acceleration peaks in conjunction with the first picket and the final laser pulse. The levels of acceleration, 200 μm/ns^2 for the first and around 600 μm/ns^2 for the second, give all reasons to believe that the dot can mix with the ablator through Rayleigh-Taylor instability, early in time ! The consequence is that the dot should dive into the ablator which would explain the anomalous position of the dot, shifted from the surface to deeper in the ablator. This effect, as we will show in the next section, is strongly inhibited in integrated simulations because of the lake of resolution to allow this effect to happen numerically.

VI. RAYLEIGH-TAYLOR MIXING OF THE DOT AND DEDICATED 2D PLANE SIMULATIONS

It is well known that in the wake of an ablation front the pressure is decreasing along with the density of the ablated material. The denser dot is pushed by the lighter ablated material. This situation gather the required conditions for a classical Rayleigh-Taylor instability (as opposed to the ablative Rayleigh-Taylor instability) given enough time to develop. Therefore, at the very beginning of the drive, the MnCo dot can potentially mix with the ablator.

In order to make this prediction more quantitative, it is important to quantify the surface roughness of a typical ablator. Depending upon the nature of the ablator, whether it is CH, HDC or beryllium, the surface roughness density spectrum (SRDS) – see Fig. 9 of Clark's[11] for typical examples – may vary but, as a rule of thumb, we can remember that above $\ell = 30$ SRDS is bellow 1 nm^2 and may be as small as 0.01 nm^2.

Now, let us call $a(\lambda, t)$ the amplitude of a given Legendre mode at time t of wavelength λ, which, for a capsule of radius R correspond to $\lambda \approx 2\pi R/\ell$. For a classical RT instability, it is well known that, in the linear regime, the amplitude of each mode grows exponentially as

$$a(\lambda, t) = a_0(\lambda)\, \exp(\sqrt{2\pi\, \mathcal{A}g/\lambda}\, t), \tag{7}$$

where $a_0(\lambda)$ is the initial amplitude. The time, $T_{\rm NL}$, it takes for such an instability to go non-linear, and beyond, is such that $a(\lambda, T_{\rm NL}) \approx \lambda$, that is to say

$$T_{\rm NL} \approx \sqrt{\lambda/(2\pi\, \mathcal{A}g)}\, \ln(\lambda/a(\lambda)). \tag{8}$$

This is why, for acceleration of order 100 μm/ns^2 – typical of the first acceleration peak in Fig.4 – this time $T_{\rm NL}$ is quite short, of order 0.1 ns for a wave length $\lambda \sim 1$ μm, even for an amplitude as small as 0.1 nm since the time varies logarithmically with amplitude.

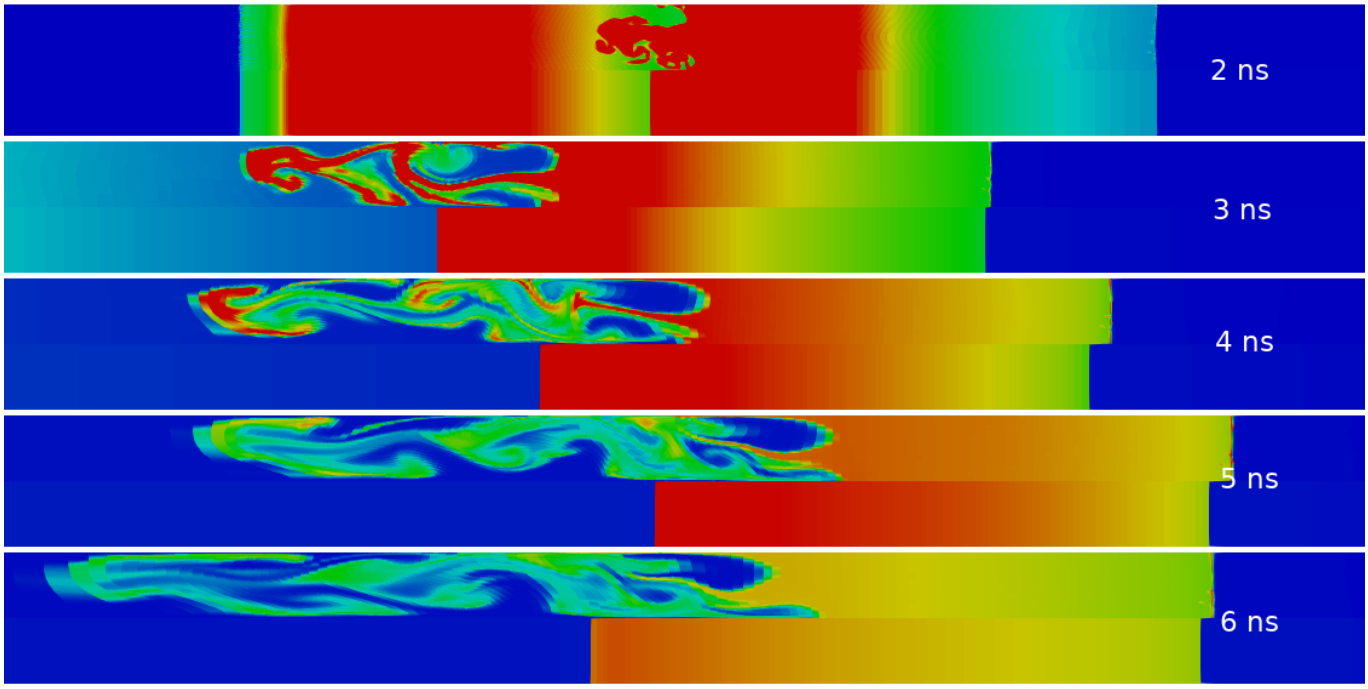

FIG. 6. (color online) Density map illustrating the mixing of the dot (from the dedicated mixing simulation: top) compared to what it would be in the integrated simulation (from the dedicated inhibited mixing simulation: down) at five different instants: 2, 3, 4, 5 and 6 ns (from top to bottom). It is clear that the dot sinks into the ablator as a result of the Rayleigh-Taylor instability due to the push of the light fluid (the ablator) onto the heavier fluid (dot of Mn:Co). X-ray flux comes from the right and the dot moves from left to right. The images have been repositioned at each instant accounting for the motion of the dot. Images, after $t = 6$ ns, are not displayed because their aspect ratio could not reasonably fit this page.

This effect can only be seen in simulations with meshes small enough to allow the instability to develop. This is not easy in an integrated simulation. Therefore, a dedicated two-dimensional plane simulation was carried out along the polar axis of the hohlraum as depicted in Fig.5. The red box correspond to the domain where the dedicated simulation is performed. The number of cells can be considerably increased in this smaller domain. The hydrodynamics boundary conditions are tailored to be representative of the actual flow (periodic at the top and bottom and free streaming on the right and left). The radiative boundary conditions are periodic at top and bottom, no incoming radiation on the left hand side. The hohlraum radiative flux, picked out of the integrated simulation, is injected on the right hand side of the simulation.

In order to be sure that this procedure reproduces the integrated motion, a deprecated version of the 2D plane simulation has been carried out. In this simulation, which is referred to as 1D, there is only one layer in the transverse direction (with respect to the axis). Thus, even if an instability should occur, it cannot develop numerically for the same reason it cannot grow in the integrated simulation. Indeed, the width of the dedicated simulation

domain is of the same order of magnitude as the size of a typical cell in the integrated simulation.

These dedicated simulations are 2D axisymmetric. 2D turbulence is well known[45] to behave differently as 3D turbulence. Even though these simulations clearly demonstrate the onset of mixing between the dot and the ablator at early time and its subsequent development, an accurate measurement of the actual 3D mixing width growth is presently out of reach for a realistic domain span of at least 100 μm (diameter of the dot) with defect as small as 500 nm.

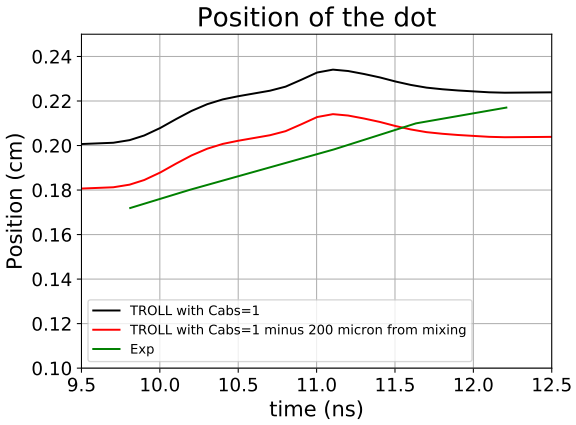

FIG. 7. Projection of the trajectory of the simulated dot if we were to take into account the possibility of mixing in 3D integrated simulations (to take into account the real dynamic of 3D mixing which is drastically different from 2D mixing).

The absolute position of the dot is shifted toward the centre due to the mixing mechanism as depicted in Fig.7. The denser MnCo dot sinks into the lighter ablator moving the absolute position of the simulated dot 200 μm closer to the experimental expected position.

Since 2D turbulence is not representative of 3D turbulence, 0D models such as buoyancy-drag model[14,18,39], well tested on 3D RT experiment, could have been used to infer what would be the actual width and position of the dot as time goes by. The problem with these 0D models is that they work well for positive time varying acceleration. As soon as acceleration changes sign, mixing increases with a slower width growth and if acceleration changes sign again the turbulent mixing zone grows unstable again but starting with an increased mixing coefficient that is to say a smaller effective Atwood number (less density contrast). There is no 0D model in the literature able to quantitatively reproduce such a complex acceleration time history. Nevertheless, it does not invalidate the formation of a mixing between the dot and the ablator. This mixing is inevitable. This has far reaching consequences on the reading of T_e from spectral line ratios as we will show in the next section.

VII. ELECTRON TEMPERATURE VERSUS LINE RATIOS INFERRED FROM A DOT MIXED WITH ABLATOR

The dot-on-capsule spectroscopy articles[2,3] assumed the dot is not mixed with the ablator. Spectral line ratios are used in a variety of context in order to infer electron temperature. If well chosen, these line ratios only depend upon electron temperature for an optically thin plasma and are, quit conveniently, only weakly sensitive[3] to electron density which is, at best, assessed by the hydrorad simulations but in no way characterized experimentally (in this dot spectroscopy platform).

Since the measurement of the absolute intensity of an emissivity spectrum is rather difficult, the ratio of the intensity I_1 and I_2 of two different spectral lines, at frequencies ν_1 and ν_2 for instance, enable to circumvent this problem. This is exactly what is done in the early dot spectroscopy experiment[2]. In more recent experiments[3], electron temperatures are not determined from line ratios but from fitting the shape of the spectra (He_α, He_β and Ly_α) for both Mn and Co.

Let us call the thickness of the dot plasma in the line of sight of the spectrometer, ℓ. If the plasma generated by the dot is optically thin at ν_1 and ν_2, that is to say, if $\kappa(\nu_1)\,\ell \ll 1$ and $\kappa(\nu_2)\,\ell \ll 1$ (where κ is the attenuation coefficient in cm^{-1} calculated from the opacity, also know as the mass attenuation coefficient, κ/ρ in cm^2/g), then I_1 and I_2 are proportional to ℓ and the ratio is independent of ℓ. On the contrary if either $\kappa(\nu_1)\,\ell$ or $\kappa(\nu_2)\,\ell$ or both are $\gg 1$, then the line ratio depends in a non trivial manner upon the thickness ℓ of the dot. In the dot, the transport of a radiation from an emissivity line at frequency ν is free streaming over distances less than $1/\kappa(\nu)$. Beyond, absorption becomes significant and can be drastically different for two neighbouring emission lines if the corresponding opacities are strong enough.

The opacity of Mn-He_α (between 6100 and 6200 eV) and Mn-Ly_α (between 6400 and 6500 eV), at T_e of few keV and $n_e \approx 10^{21}$ cm^{-3} (typical of the dot between 10 and 12 ns), are respectively of order $(\kappa/\rho) \approx 10^5$ cm^2/g and $(\kappa/\rho) \approx 10^4$ cm^2/g (cf. Fig.8). That value of n_e correspond to a density of order $\rho \approx 10^{-3}$ g/cm^3 for Mn. The attenuation coefficient for Mn-He_α is therefore of order 10^2 cm^{-1} since $\kappa = (\kappa/\rho) \times \rho = 10^5 \times 10^{-3} = 10^2$ cm^{-1} and it is of order 10 cm^{-1} for Mn-Ly_α since $\kappa = (\kappa/\rho) \times \rho = 10^4 \times 10^{-3} = 10$ cm^{-1}. They correspond to mean free paths of order $1/\kappa \approx 10^{-2}$ cm, that is to say 100 μm for Mn-He_α and $1/\kappa \approx 10^{-1}$ cm, that is to say 1 mm, for Mn-Ly_α. This is the reason why for a dot of thickness of order 100 μm, precise measurement of T_e requires precise measurement of the thickness of the dot along the line of sight of the spectrometer. Widths of hundreds of microns do not affect the intensity of Mn-Ly_α, with a mean free path of order 1000 μm, but they attenuate significantly (with increasing width) the intensity of Mn-He_α , with a mean free path of order 100 μm. Therefore, as width increases, the line ratio Mn-Ly_α over

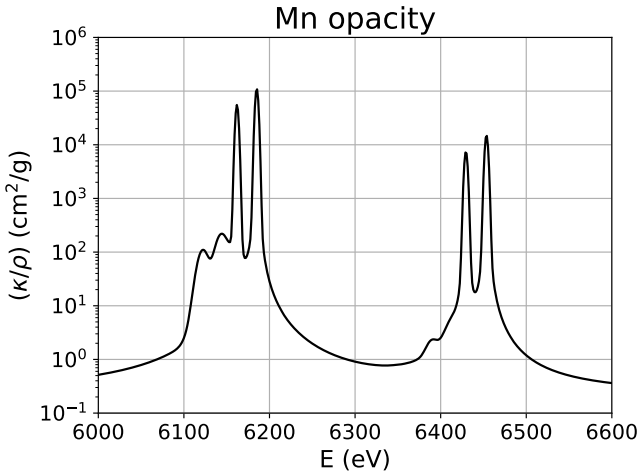

FIG. 8. Opacity for a plasma of Mn between 6.0 and 6.6 keV for $n_e = 10^{21}$ cm^{-3}, $T_e = T_i = 4.0$ keV and $T_r = 300$ eV typical of the dot spectroscopy experiment during the interval of measurement.

Mn-He$_\alpha$ increases for the same electron temperature or, which is equivalent, the electron temperature decreases for the same ratio Mn-Ly$_\alpha$ over Mn-He$_\alpha$. It explains the trends reported on Fig.9.

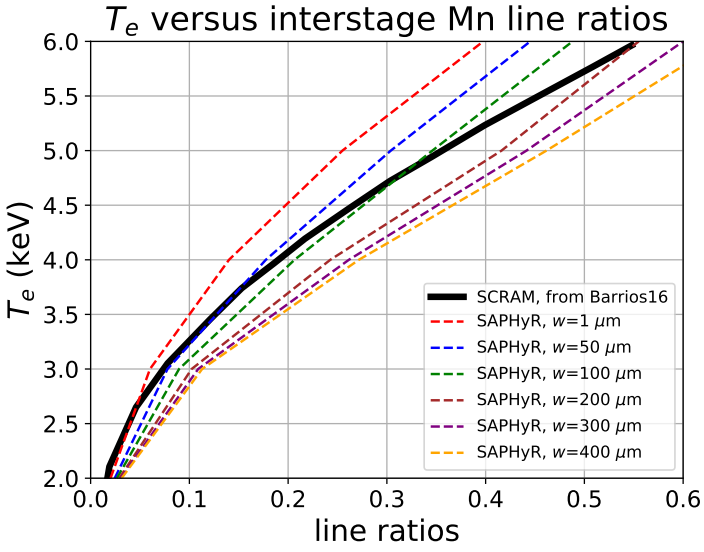

FIG. 9. $\frac{Mn-Ly_\alpha}{Mn-He_\alpha}$ interstage ratios versus electronic temperature for thicknesses varying from 1 to 400μm, as calculated by SAPHyR (black lines) and as calculated by SCRAM[2], the red line.

Needless to say that, if on top of that, one takes into account mixing of the dot with the ablator, the problem is even more complicated because not only is the thickness required to get an accurate indirect measurement of T_e but the density profile too is needed because mixing makes it non uniform which complicates yet further the calculation of the line ratio.

In the remaining of this section, only the effect of the dot width on the T_e measurement will be assessed.

A stationary collisional-radiative (CR) model, SAPHyR, has been used to calculate the spectral intensity of non-LTE Mn plasma. Following references[10,17,43], the atomic structure is described in term of superconfiguration (SC) defined by an integer filling of shells, here characterized by principal quantum numbers.

For each ionic stage, only are retained the ground SC and excited SCs resulting on the promotion, when it is possible, of one and two electrons from K- and L-shells of the ground SC to upper shells (up to n=10). In the present work, fully stripped ion up to C-like ionic stages have been considered. All the atomic data needed for the CR model are calculated from a non-relativistic quantum-mechanical formalism[37]. Electron impact collisional ionization (excitation), photo-ionization (excitation) and autoionization processes are considered. Relativistic microreversibility relations are used to evaluate all transition rates needed[16]. Because large plasma thicknesses are considered in the present work, the effect of opacity on the radiative rates need to be included. Such effect is treated here using an escape factor approximation[36]. Although density effects are negligible in the present work, the Stewart-Pyatt model[44] is used to describe the pressure ionization. The SC populations are computed using a coupled set of rate equations and once obtained, a full configuration splitting is performed. These SC populations occurrence probabilities are deduced from the Boltzmann law using the electron temperature. Spectral opacity and emissivity are then calculated using the spectral module of the OPAS code[7], modified to compute opacity and emissivity of non-LTE plasmas.

The ratio (R) of spectrally integrated intensities is shown in Fig.9. Spectral intensity is given by

$$I_\nu = \frac{\epsilon_\nu}{\kappa_\nu}(1 - e^{\kappa_\nu \rho \ell}), \tag{9}$$

where $\epsilon_\nu(\kappa_\nu)$ is the frequency resolved emissivity (opacity), ρ the mass density, and ℓ the thickness. The numerator of this ratio corresponds to the integration range 6.35-6.45 keV of the Ly_α lines (including He-like satellites) while the denominator corresponds to the integration range 6.1-6.2 keV of the He_α lines (including Li-like satellites). Note that the ratio defined as above is not a real interstage line ratio because not only one electron state nor two-electron state of the plasma are considered for the Ly_α lines and the He_α lines, respectively. Such large integration ranges have been retained to mimic experimental conditions[2].

Calculations have been performed for electron density $n_e = 10^{21}$ cm^{-3} (see Fig.10) and for electron temperatures T_e in the range 2-6 keV using a 1 keV step (see Fig.11).

Radiation field has been ignored. Six plasma thicknesses values have been considered : 1, 50, 100, 200,

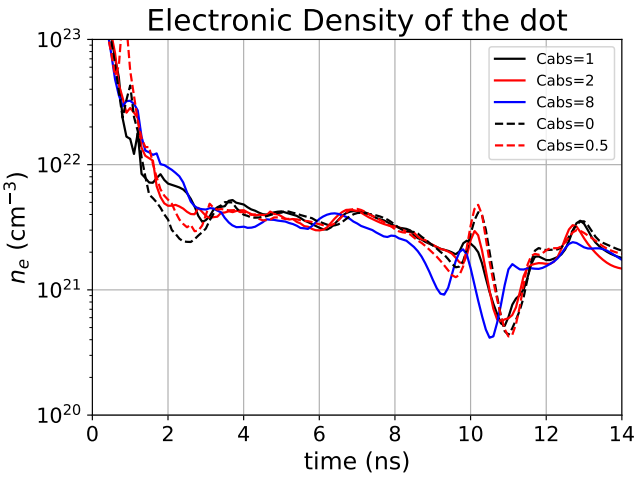

FIG. 10. History of electronic density ($n_e(t)$) of the dot.

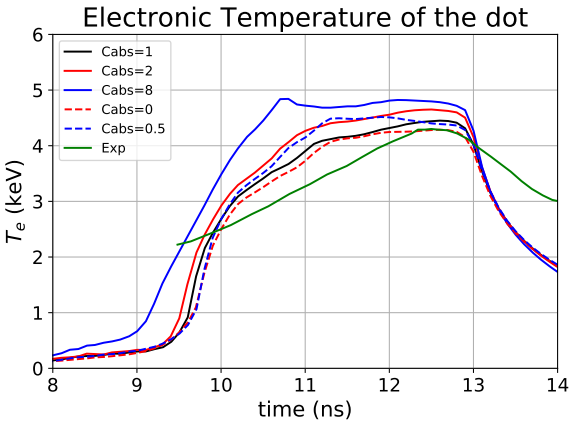

FIG. 11. Electronic temperature in the dot versus time. Peak T_e is consistent with C_{abs} around 1 (from 0. to 1.) in the gas-fill.

300, and 400 μm. For each thickness, the ratio R versus T_e has been fitted using a simple parabolic function $R = aT_e^2 + bT_e + c$. Using these fits, we can calculate the relative uncertainties on T_e values inferred from given values of R for all thicknesses. A summary is shown in the Table VII. If the thickness is taken into account in the calculation, the uncertainty can be as high as 25% on the inferred values of T_e. This could be of the highest concern if the dot-ablator mixture thickness is not very well estimated and/or affected by instability during expansion. In the Table VII, in the same way we show the estimation of the relative uncertainty on T_e if inferred from ratios associated with a $\pm 10\%$ error. The uncertainty increases when the ratio (that is T_e) and/or the thickness grow from 6% (e.g. e=400μm/$R = 0.1$) to nearly 10% (e=200μm/$R = 0.4$).

R (Ly_α/He_α)	0.1	0.2	0.3	0.4
$Te_{(e=1\mu m)} - Te_{(e=400\mu m)}(keV)$	0.8	1.06	1.18	1.24
$\frac{\Delta Te}{Te}$	26%	26%	25%	23%

TABLE II. Absolute and relative electron temperature values inferred from Ly_α/He_α ratios equal to 0.1, 0.2, 0.3 and 0.4 when thickness varies from 1 to 400μm.

R (Ly_α/He_α)	0.1	0.2	0.3	0.4
$Te_{(R+10\%)} - Te_{(R-10\%)}(keV)$	0.153	0.35	0.43	0.49
$e = 1\mu m$	7.2%	7.7%	7.9%	8.1%
$e = 50\mu m$	7.5%	8.4%	8.8%	9%
$e = 100\mu m$	7.3%	8.7%	9.2%	9.5%
$e = 200\mu m$	6.7%	8.5%	9.3%	9.8%
$e = 300\mu m$	6.4%	8.3%	9.2%	9.6%
$e = 400\mu m$	6.2%	8.1%	9%	9.5%

TABLE III. Absolute and relative electron temperature variations ($\frac{\Delta T_e}{T_e}$) inferred from variation around Ly_α/He_α ratios of $\pm 10\%$ around 0.1, 0.2, 0.3 and 0.4, for given plasma thickness.

VIII. CONCLUSION

Integrated simulations of the dot spectroscopy experiment[2,3] with CEA hydro-radiation code TROLL has shown similar results than HYDRA, LLNL hydro-radiation code, that is to say, a systematic overestimation of the position of the dot.

The new *absorption multipliers*, that has been implemented in TROLL, showed that even strong and sometimes unphysical alteration of absorption mechanism, keeping the energy budget in the cavity all the same, did not affect the trajectory until late time and, even then, the modification was not enough to explain a significant part of the difference. This led us to investigate early causes of this discrepancy.

Simulations of the dot region with finer mesh have demonstrated a Rayleigh-Taylor mixing of the dot with the ablator as it expands in the hohlraum. It was triggered at the first instants of ablation, very early in the experiment.

Not only does this effect explain a significant part of the trajectory shift between integrated simulations and experiment but it raises the unexpected issue of the indirect measurement of electron temperature (the very reason of the dot platform on NIF) with line ratios of Mn and Co in a mixed dot. The relation between electron temperature and these line ratios has shown to be strongly influenced by the width of the dot in hohlraum conditions (involving width of hundreds of microns). This is so regardless of any mixing, but mixing makes it even more difficult to infer because the density profile of Mn and Co, which is not uniform anymore in a mixing, should be assessed in order to properly relates electron temperature to line ratios.

ACKNOWLEDGMENTS

The authors would like to acknowledge O. Morice, from CEA, for having dealt with the *absorption multipliers* in the hydro-rad code TROLL[27]. The authors would also like to acknowledge D. A. Callahan and D. Hinkel, from Lawrence Livermore National Laboratory, for providing us with the necessary data to carry out our own simulations of the dot experiment with the hydro-rad code TROLL.

DATA AVAILABILITY

The data that support the findings of this study are available from the corresponding author upon reasonable request.

REFERENCES

[1]S. J. Ali, P. M. Celliers, S. W. Haan, T. R. Boehly, N. Whiting, S. H. Baxamusa, H. Reynolds, M. A. Johnson, J. D. Hughes, B. Watson, K. Engelhorn, V. A. Smalyuk, and O. L. Landen. Hydrodynamic instability seeding by oxygen nonuniformities in glow discharge polymer inertial fusion ablators. *Phys. Rev. E*, 98:033204, Sep 2018.

[2]M. A. Barrios, D. A. Liedahl, M. B. Schneider, O. Jones, G. V. Brown, S. P. Regan, K. B. Fournier, A. S. Moore, J. S. Ross, O. Landen, R. L. Kauffman, A. Nikroo, J. Kroll, J. Jaquez, H. Huang, S. B. Hansen, D. A. Callahan, D. E. Hinkel, D. Bradley, and J. D. Moody. Electron temperature measurements inside the ablating plasma of gas-filled hohlraums at the national ignition facility. *Phys. Plasmas*, 23:056307, 2016.

[3]M. A. Barrios, J. D. Moody, L. J. Suter, M. Sherlock, H. Chen, W. Farmer, J. Jaquez, O. Jones, R. L. Kauffman, J. D. Kilkenny, J. Kroll, O. L. Landen, D. A. Liedahl, S. A. Maclaren, N. B. Meezan, A. Nikroo, M. B. Schneider, D. B. Thorn, K. Widmann, and G. Pérez-Callejo. Developing an experimental basis for understanding transport in nif hohlraum plasmas. *Phys. Rev. Lett.*, 121:095002, Aug 2018.

[4]L. F. Berzak Hopkins, S. Le Pape, L. Divol, N. B. Meezan, A. J. Mackinnon, D. D. Ho, O. S. Jones, S. Khan, J. L. Milovich, J. S. Ross, P. Amendt, D. Casey, P. M. Celliers, A. Pak, J. L. Peterson, J. Ralph, and J. R. Rygg. Near-vacuum hohlraums for driving fusion implosions with high density carbon ablators. *Phys. Plasmas*, 22(5):056318, May 2015.

[5]L. F. Berzak Hopkins, S. Le Pape, L. Divol, N. B. Meezan, A. J. Mackinnon, D. D. Ho, O. S. Jones, S. Khan, J. L. Milovich, J. S. Ross, P. Amendt, D. Casey, P. M. Celliers, A. Pak, J. L. Peterson, J. Ralph, and J. R. Rygg. Near-vacuum hohlraums for driving fusion implosions with high density carbon ablators. *Physics of Plasmas*, 22(5):056318, 2015.

[6]L. F. Berzak Hopkins, N. B. Meezan, S. Le Pape, L. Divol, A. J. Mackinnon, D. D. Ho, M. Hohenberger, O. S. Jones, G. Kyrala, J. L. Milovich, A. Pak, J. E. Ralph, J. S. Ross, L. R. Benedetti, J. Biener, R. Bionta, E. Bond, D. Bradley, J. Caggiano, D. Callahan, C. Cerjan, J. Church, D. Clark, T. Doppner, R. Dylla-Spears, M. Eckart, D. Edgell, J. Field, D. N. Fittinghoff, M. Gatu Johnson, G. Grim, N. Guler, S. Haan, A. Hamza, E. P. Hartouni, R. Hatarik, H. W. Herrmann, D. Hinkel, D. Hoover, H. Huang, N. Izumi, S. Khan, B. Kozioziemski, J. Kroll, T. Ma, A. MacPhee, J. McNaney, F. Merrill, J. Moody, A. Nikroo, P. Patel, H. F. Robey, J. R. Rygg, J. Sater, D. Sayre, M. Schneider, S. Sepke, M. Stadermann, W. Stoeffl, C. Thomas, R. P. J. Town, P. L. Volegov, C. Wild, C. Wilde, E. Woerner, C. Yeamans, B. Yoxall, J. Kilkenny, O. L. Landen, W. Hsing, and M. J. Edwards. First high-convergence cryogenic implosion in a near-vacuum hohlraum. *Phys. Rev. Lett.*, 114:175001, April 2015.

[7]C. Blancard, P. Cosse, and G. Faussurier. Solar mixture opacity calculations using detailed configuration and level accounting treatments. *Astrophys. J.*, 745:10, 2012.

[8]A. Casner, C. Mailliet, G. Rigon, S.F. Khan, D. Martinez, B. Albertazzi, T. Michel, T. Sano, Y. Sakawa, P. Tzeferacos, D. Lamb, S. Liberatore, N. Izumi, D. Kalantar, P. Di Nicola, J.M. Di Nicola, E. Le Bel, I. Igumenshchev, V. Tikhonchuk, B.A. Remington, J. Ballet, E. Falize, L. Masse, V.A. Smalyuk, and M. Koenig. From ICF to laboratory astrophysics: ablative and classical rayleigh–taylor instability experiments in turbulent-like regimes. *Nucl. Fusion*, 59(3):032002, dec 2018.

[9]A. R. Christopherson, R. Betti, and J. D. Lindl. Thermonuclear ignition and the onset of propagating burn in inertial fusion implosions. *Phys. Rev. E*, 99:021201, Feb 2019.

[10]H.-K. Chung, M.H. Chen, W.L. Morgan, Y. Ralchenko, and R.W. Lee. Flychk: Generalized population kinetics and spectral model for rapid spectroscopic analysis for all elements. *High Energy Dens. Phys.*, 1(1):3 – 12, October 2005.

[11]D. S. Clark, A. L. Kritcher, S. A. Yi, A. B. Zylstra, S. W. Haan, and C. R. Weber. Capsule physics comparison of national ignition facility implosion designs using plastic, high density carbon, and beryllium ablators. *Phys. Plasmas*, 25(3):032703, March 2018.

[12]P. Colin-Lalu, V. Recoules, G. Salin, and G. Huser. Impact of oxygen on the 300-k isotherm of laser megajoule ablator using ab initio simulation. *Phys. Rev. E*, 92:053104, November 2015.

[13]C. Courtois, O. Poujade, E. Alozy, S. Brygoo, C. Chicanne, T. Chies, S. Darbon, A. Duval, J. Fariaut, M. Ferri, H. Graillot, O. Henry, B. Marchet, I. Masclet-Gobin, P. Seytor, G. Soullie, L. Videau, B. Villette, and R. Wrobel. First experimental observation of a photoabsorption-edge induced shock by its coalescence onto a regular ablation-shock. *Phys. Plasmas*, 27:042702, 2020.

[14]Guy Dimonte. Spanwise homogeneous buoyancy-drag model for rayleigh-taylor mixing and experimental evaluation. *Phys. Plasmas*, 7(6):2255, December 2000.

[15]W A Farmer, O S Jones, M A Barrios, D J Strozzi, J M Koning, G D Kerbel, D E Hinkel, J D Moody, L J Suter, D A Liedahl, N Lemos, D C Eder, R L Kauffman, O L Landen, A S Moore, and M B Schneider. Heat transport modeling of the dot spectroscopy platform on NIF. *Plasma Physics and Controlled Fusion*, 60(4):044009, feb 2018.

[16]Gérald Faussurier and Christophe Blancard. Degeneracy and relativistic microreversibility relations for collisional-radiative equilibrium models. *Phys. Rev. E*, 95:063201, June 2017.

[17]Franck Gilleron and Robin Piron. The fast non-lte code dedale. *High Energy Dens. Phys.*, 17, Part B:219 – 230, July 2015.

[18]Benoit-Joseph Grea, Alan Burlot, Jerome Griffond, and Antoine Llor. Challenging mix models on transients to self-similarity of unstably stratified homogeneous turbulence. *J Fluids Eng*, 138:070904, 2016.

[19]Brian M. Haines, R. E. Olson, W. Sweet, S. A. Yi, A. B. Zylstra, P. A. Bradley, F. Elsner, H. Huang, R. Jimenez, J. L. Kline, C. Kong, G. A. Kyrala, R. J. Leeper, R. Paguio, S. Pajoom, R. R. Peterson, M. Ratledge, and N. Rice. Robustness to hydrodynamic instabilities in indirectly driven layered capsule implosions. *Phys. Plasmas*, 26(1):012707, January 2019.

[20]O. A. Hurricane, D. A. Callahan, and C. Cerjan E. L. Dewald T. R. Dittrich T. Doppner D. E. Hinkel L..F. Berzak Hopkins J. L. Kline S. Le Pape T. Ma A. G. MacPhee J. L. Milovich A. Pak H.-S. Park P. K. Patel B. A. Remington J. D. Salmonson P. T. Springer D. T. Casey, P. M. Celliers. Fuel gain exceeding unity in an inertially confined fusion implosion. *Nature*, page 343, February 2014.

[21]O. A. Hurricane, P. T. Springer, P. K. Patel, D. A. Callahan, K. Baker, D. T. Casey, L. Divol, T. Doppner, D. E. Hinkel, M. Hohenberger, L. F. Berzak Hopkins, C. Jarrott, A. Kritcher, S. Le Pape, S. Maclaren, L. Masse, A. Pak, J. Ralph, C. Thomas,

P. Volegov, and A. Zylstra. Approaching a burning plasma on the nif. *Phys. Plasmas*, 26(5):052704, May 2019.

[22]G. Huser, V. Recoules, N. Ozaki, T. Sano, Y. Sakawa, G. Salin, B. Albertazzi, K. Miyanishi, and R. Kodama. Experimental and ab initio investigations of microscopic properties of laser-shocked ge-doped ablator. *Phys. Rev. E*, 92:063108, December 2015.

[23]O. S. Jones, C. J. Cerjan, M. M. Marinak, J. L. Milovich, H. F. Robey, P. T. Springer, L. R. Benedetti, D. L. Bleuel, E. J. Bond, D. K. Bradley, D. A. Callahan, J. A. Caggiano, P. M. Celliers, D. S. Clark, S. M. Dixit, T. Doppner, R. J. Dylla-Spears, E. G. Dzentitis, D. R. Farley, S. M. Glenn, S. H. Glenzer, S. W. Haan, B. J. Haid, C. A. Haynam, D. G. Hicks, B. J. Kozioziemski, K. N. LaFortune, O. L. Landen, E. R. Mapoles, A. J. MacKinnon, J. M. McNaney, N. B. Meezan, P. A. Michel, J. D. Moody, M. J. Moran, D. H. Munro, M. V. Patel, T. G. Parham, J. D. Sater, S. M. Sepke, B. K. Spears, R. P. J. Town, S. V. Weber, K. Widmann, C. C. Widmayer, E. A. Williams, L. J. Atherton, M. J. Edwards, J. D. Lindl, B. J. MacGowan, L. J. Suter, R. E. Olson, H. W. Herrmann, J. L. Kline, G. A. Kyrala, D. C. Wilson, J. Frenje, T. R. Boehly, V. Glebov, J. P. Knauer, A. Nikroo, H. Wilkens, and J. D. Kilkenny. A high-resolution integrated model of the national ignition campaign cryogenic layered experimentsa). *Phys. Plasmas*, 19(5):056315, May 2012.

[24]O. S. Jones, L. J. Suter, H. A. Scott, M. A. Barrios, W. A. Farmer, S. B. Hansen, D. A. Liedahl, C. W. Mauche, A. S. Moore, M. D. Rosen, J. D. Salmonson, D. J. Strozzi, C. A. Thomas, and D. P. Turnbull. Progress towards a more predictive model for hohlraum radiation drive and symmetry. *Physics of Plasmas*, 24(5):056312, 2017.

[25]R K Kirkwood, J D Moody, J Kline, E Dewald, S Glenzer, L Divol, P Michel, D Hinkel, R Berger, E Williams, J Milovich, L Yin, H Rose, B MacGowan, O Landen, M Rosen, and J Lindl. A review of laser-plasma interaction physics of indirect-drive fusion. *Plasma Phys. Control. Fusion*, 55:103001, September 2013.

[26]A. Bruce Langdon. Nonlinear inverse bremsstrahlung and heated-electron distributions. *Phys. Rev. Lett.*, 44:575, 1980.

[27]E. Lefebvre, S. Bernard, C. Esnault, P. Gauthier, A. Grisollet, P. Hoch, L. Jacquet, G. Kluth, S. Laffite, S. Liberatore, I. Marmajou, P.-E. Masson-Laborde, O. Morice, and J.-L. Willien. Development and validation of the TROLL radiation-hydrodynamics code for 3d hohlraum calculations. *Nucl. Fusion*, 59(3):032010, dec 2018.

[28]J. D. Lindl, S. W. Haan, O. L. Landen, A. R. Christopherson, and R. Betti. Progress toward a self-consistent set of 1d ignition capsule metrics in icf. *Phys. Plasmas*, 25(12):122704, December 2018.

[29]John Lindl, Otto Landen, John Edwards, Ed Moses, and NIC Team. Review of the national ignition campaign 2009-2012. *Phys. Plasmas*, 21(2):020501, February 2014.

[30]A. MacLaren, S. B. Schneider, M. K. Widmann, H. Hammer, J. E. Yoxall, B. D. Moody, J. M. Bell, P. R. Benedetti, L. K. Bradley, D. J. Edwards, M. M. Guymer, T. E. Hinkel, D. W. Hsing, W. L. Kervin, M. B. Meezan, N. S. Moore, A. and E. Ralph, J.˙Novel characterization of capsule x-ray drive at the national ignition facility. *Phys. Rev. Lett.*, 112:105003, March 2014.

[31]A. G. MacPhee, V. A. Smalyuk, O. L. Landen, C. R. Weber, H. F. Robey, E. L. Alfonso, K. L. Baker, L. F. Berzak Hopkins, J. Biener, T. Bunn, D. T. Casey, D. S. Clark, J. W. Crippen, L. Divol, M. Farrell, S. Felker, J. E. Field, W. W. Hsing, C. Kong, S. Le Pape, D. A. Martinez, P. Michel, J. Milovich, A. Moore, A. Nikroo, L. Pickworth, N. Rice, M. Stadermann, C. Yeamans, and C. Wild. Hydrodynamic instabilities seeded by the x-ray shadow of icf capsule fill-tubes. *Phys. Plasmas*, 25(8):082702, August 2018.

[32]J. D. Moody, D. A. Callahan, D. E. Hinkel, P. A. Amendt, K. L. Baker, D. Bradley, P. M. Celliers, E. L. Dewald, L. Divol, T. Doppner, D. C. Eder, M. J. Edwards, O. Jones, S. W. Haan, D. Ho, L. B. Hopkins, N. Izumi, D. Kalantar, R. L. Kauffman, J. D. Kilkenny, O. Landen, B. Lasinski, S. LePape, T. Ma, B. J. MacGowan, S. A. MacLaren, A. J. Mackinnon, D. Meeker, N. Meezan, P. Michel, J. L. Milovich, D. Munro, A. E. Pak, M. Rosen, J. Ralph, H. F. Robey, J. S. Ross, M. B. Schneider, D. Strozzi, E. Storm, C. Thomas, R. P. J. Town, K. L. Widmann, J. Kline, G. Kyrala, A. Nikroo, T. Boehly, A. S. Moore, and S. H. Glenzer. Progress in hohlraum physics for the national ignition facility. *Phys. Plasmas*, 21(5):056317, May 2014.

[33]R. M. More, K. H. Warren, D. A. Young, and G. B. Zimmerman. A new quotidian equation of state (qeos) for hot dense matter. *Physics of Fluids*, 31:3059, 1988.

[34]F. Perez, G. E. Kemp, S. P. Regan, M. A. Barrios, J. Pino, H. Scott, S. Ayers, H. Chen, J. Emig, J. D. Colvin, M. Bedzyk, M. J. Shoup, A. Agliata, B. Yaakobi, F. J. Marshall, R. A. Hamilton, J. Jaquez, M. Farrell, A. Nikroo, and K. B. Fournier. The nif x-ray spectrometer calibration campaign at omega. *Rev. Sci. Instrum.*, 85(11), July 2014.

[35]J. R. Peterson, B. M. Johnson, and S. W. Haan. Instability growth seeded by dt density perturbations in icf capsules. *Phys. Plasmas*, 25(9):092705, 2018.

[36]G.J. Phillips, J.S. Wark, F.M. Kerr, S.J. Rose, and R.W. Lee. Escape factors in zero-dimensional radiation-transfer codes. *High Energy Dens. Phys.*, 4:18, 2008.

[37]M.S. Pindzola, D.C. Griffin, and C. Bottcher. *Atomic Processes in Electron-Ion and Ion-Ion Collisions, NATO Advanced Study Institute, Series B: Physics, Plenum, New York.* 1986.

[38]O. Poujade, M. Ferri, and I. Geoffray. New radiographic image processing tested on the simple and double-flux platform at omega. *Physics of Plasmas*, 24(10):102105, October 2017.

[39]O. Poujade and M. Peybernes. Growth rate of rayleigh-taylor turbulent mixing layers with the foliation approach. *Phys. Rev. E*, 81:016316, 2010.

[40]Hans G Rinderknecht, P A Amendt, S C Wilks, and G Collins. Kinetic physics in icf: present understanding and future directions. *Plasma Physics and Controlled Fusion*, 60:064001, 2018.

[41]H. F. Robey, T. R. Boehly, P. M. Celliers, J. H. Eggert, D. Hicks, R. F. Smith, R. Collins, M. W. Bowers, K. G. Krauter, P. S. Datte, D. H. Munro, J. L. Milovich, O. S. Jones, P. A. Michel, C. A. Thomas, R. E. Olson, S. Pollaine, R. P. J. Town, S. Haan, D. Callahan, D. Clark, J. Edwards, J. L. Kline, S. Dixit, M. B. Schneider, E. L. Dewald, K. Widmann, J. D. Moody, T. Doppner, H. B. Radousky, A. Throop, D. Kalantar, P. DiNicola, A. Nikroo, J. J. Kroll, A. V. Hamza, J. B. Horner, S. D. Bhandarkar, E. Dzenitis, E. Alger, E. Giraldez, C. Castro, K. Moreno, C. Haynam, K. N. LaFortune, C. Widmayer, M. Shaw, K. Jancaitis, T. Parham, D. M. Holunga, C. F. Walters, B. Haid, E. R. Mapoles, J. Sater, C. R. Gibson, T. Malsbury, J. Fair, D. Trummer, K. R. Coffee, B. Burr, L. V. Berzins, C. Choate, S. J. Brereton, S. Azevedo, H. Chandrasekaran, D. C. Eder, N. D. Masters, A. C. Fisher, P. A. Sterne, B. K. Young, O. L. Landen, B. M. Van Wonterghem, B. J. MacGowan, J. Atherton, J. D. Lindl, D. D. Meyerhofer, and E. Moses. Shock timing experiments on the national ignition facility: Initial results and comparison with simulation. *Phys. Plasmas*, 19:042706, April 2012.

[42]M. B. Schneider, S. A. MacLaren, K. Widmann, N. B. Meezan, J. H. Hammer, B. E. Yoxall, P. M. Bell, L. R. Benedetti, D. K. Bradley, D. A. Callahan, E. L. Dewald, T. Doppner, D. C. Eder, M. J. Edwards, T. M. Guymer, D. E. Hinkel, M. Hohenberger, W. W. Hsing, M. L. Kervin, J. D. Kilkenny, O. L. Landen, J. D. Lindl, M. J. May, P. Michel, J. L. Milovich, J. D. Moody, A. S. Moore, J. E. Ralph, S. P. Regan, C. A. Thomas, and A. S. Wan. The size and structure of the laser entrance hole in gas-filled hohlraums at the national ignition facility. *Phys. Plasmas*, 22(12):122705, December 2015.

[43]H.A. Scott and S.B. Hansen. Advances in nlte modeling for integrated simulations. *High Energy Dens. Phys..*, 6(1):39, August 2010.

[44]John C. Stewart and Jr. Kedar D. Pyatt. Lowering of ionization potentials in plasmas. *Astrophysical Journal*, 144:1203, 1966.

[45]Patrick Tabeling. Two-dimensional turbulence: a physicist approach. *Phys. Rep.*, 362:1–62, 2002.

[46] V.T. Tikhonchuk. Physics of laser plasma interaction and particle transport in the context of inertial confinement fusion. *Nucl. Fusion*, 59(3):032001, dec 2018.

[47] D. Turnbull, L. F. Berzak Hopkins, S. Le Pape, L. Divol, N. Meezan, O. L. Landen, D. D. Ho, A. Mackinnon, A. B. Zylstra, H. G. Rinderknecht, H. Sio, R. D. Petrasso, J. S. Ross, S. Khan, A. Pak, E. L. Dewald, D. A. Callahan, O. Hurricane, W. W. Hsing, and M. J. Edwards. Symmetry control in subscale near-vacuum hohlraums. *Physics of Plasmas*, 23(5):052710, 2016.

[48] Ye Zhou. Rayleigh–taylor and richtmyer–meshkov instability induced flow, turbulence, and mixing. i. *Physics Reports*, 720-722:1–136, 2017.